

Flexible Exoskeletons for Magnetically Actuated Microscopic Robots using Atomic Layer Deposition

CNF Project Number: 900-00

Principal Investigator(s): Paul L. McEuen^{1,2}, Itai Cohen^{1,2}

User(s): Tanner Pearson³, Kyle Dorsey³, Edward Esposito¹, Sierra Russell⁴, Baris Bircan³

Affiliation(s): 1. Laboratory of Atomic and Solid State Physics, Cornell University; 2. Kavli Institute for Nanoscale Science, Cornell University; 3. School of Applied and Engineering Physics, Cornell University; 4. College of Nanoscale Sciences, SUNY Polytechnic Institute

Primary Source(s) of Research Funding: This work was supported by National Science Foundation (NSF) grant DMR-1435829, Air Force Office of Scientific Research (AFSOR) multidisciplinary research program of the university research initiative grant FA2386-13-1-4118, Cornell Center for Materials Research (CCMR) through NSF MRSEC program (DMR-1719875), ARO grant W911NF-18-1-0032, NSF Major Research Instrumentation Award DMR-1429155, the National Science Foundation under Grant No. NNCI-1542081, and the Kavli Institute at Cornell for Nanoscale Science

Contact: plm23@cornell.edu, itai.cohen@cornell.edu, tgp34@cornell.edu, kjd96@cornell.edu, epe3@cornell.edu, srussell@sunypoly.edu, bb625@cornell.edu

Primary CNF Tools Used: Oxford FlexAL ALD, Arradiance ALD, Autostep AS200 i-line stepper, CVC e-beam evaporators, Oxford 81/82 etchers, PT770/PT740 etchers, Anatech Asher, Zeiss SEMs, Veeco AFM, Tencor P7 profilometer, FilmMetrics UV, Woollam ellipsometer, DISCO dicing saw, Heidelberg DWL2000, AJA sputterer

Abstract:

One of the grand challenges in robotics is to create truly microscopic robots, i.e. those too small to be resolved by the naked eye. We attack this problem by combining programmable magnetic panels with nanometer-thick flexible materials to make micron-scale, magnetically controlled robots and smart assemblies. The ideal material for this flexible exoskeleton must be elastic, possess high intrinsic strength, and integrate easily into standard microfabrication processes. We employ atomic layer deposition (ALD) to synthesize films down to 2 nm thickness to create membranes, metamaterials, and machines [1]. We demonstrate that these ALD films behave elastically under repeated deformation and have fJ-scale bending stiffness. We further incorporate magnetic panels to controllably actuate simple mechanisms and machines. These results establish ultrathin ALD films as flexible materials for microscopic actuating systems. Our current pursuit focuses on improving functionality of these systems by encoding them with magnetic information. This idea can be implemented to program dipole orientations in individual magnetic panels, enabling more complex modes of actuation for executing specific tasks [2]. Moreover, patterned magnetic multipoles can be utilized for smart self-assembly via specific binding [3]. Ultimately, the use of magnetic programming techniques to design actuating systems based on ALD films will provide a unique platform for constructing and manipulating microscopic robotic systems.

Summary of Research:

ALD is an ideal technique for scaling mechanical systems to micron-scale dimensions. We have developed an entire fabrication strategy around ALD, including lithography, etching, release, and integration. ALD films are grown conformally on a sacrificial layer of aluminum, as shown schematically in Figure 1. The devices consist of lithographically patterned regions of ALD membranes and thicker panels of other materials that provide rigid structure and additional functions such as mirrors or magnets. The devices are fabricated at wafer scales at yields exceeding 90%. The wafer is diced and devices are released by immersing in dilute base, followed by rinsing in water. Upon release, all experiments are

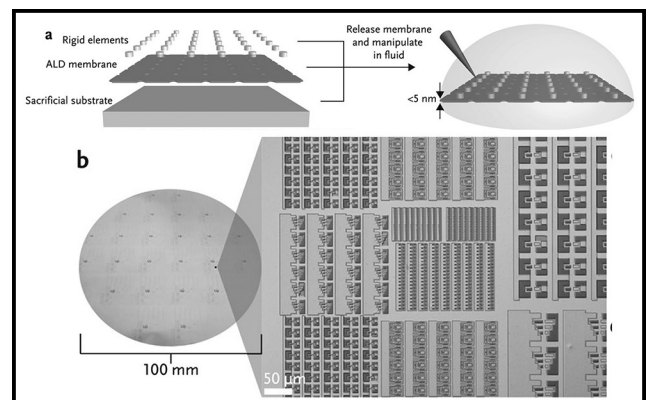


Figure 1: (a) Schematic of the fabrication and release processes. (b) Photograph of a 100 mm wafer with myriad ALD devices.

carried out in aqueous environments, often with added surfactant, to avoid stiction of the free membranes.

We investigated the mechanical properties of these films by measuring the bending stiffness of over 60 magnetically actuated glass hinges. Ferromagnets with saturated in-plane moments are patterned on panels at the ends of the hinges. The panels are deflected when we apply an out-of-plane magnetic field B , and the bending stiffness is determined by measuring the corresponding deflections of the hinges. Scaling the thickness from 2 nm to 8 nm, we find bending stiffnesses spanning nearly two orders of magnitude, with the lowest being in the femtojoule range. We additionally find the Young's modulus of ALD glass to be 90 ± 10 GPa. This value is comparable to values for bulk material (70-80 GPa), indicating that even at 2 nm thickness, the films behave mechanically similar to macroscopic counterparts.

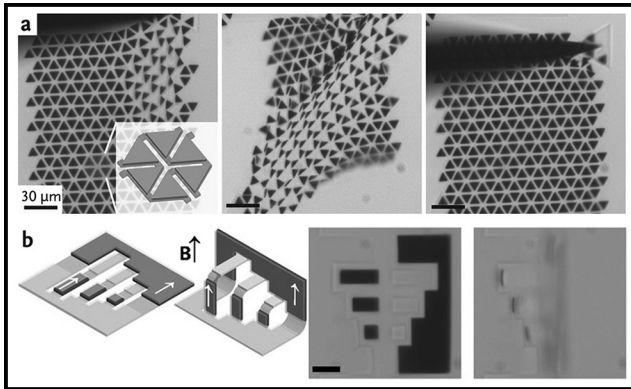


Figure 2: (a) Biaxially stretchable mechanical metamaterial. (b) Magnetically actuated pop-up staircase.

We additionally use ALD membranes to fabricate a range of microscopic actuatable systems (Figure 2). Glass and platinum sheets can be patterned into geometries that allow parts of the sheet to bend/buckle out of its fabrication plane, producing highly stretchable and auxetic metamaterials. Moreover, ferromagnetic panels can be introduced to create magnetically actuated machines that function with exquisitely small forces and torques. These span from pop-up book style devices that can be snapped shut, to muscle mimetic load bearing mechanisms.

Our recent efforts focus on improving functionality of these actuatable systems by encoding them with magnetic information. This idea can be implemented

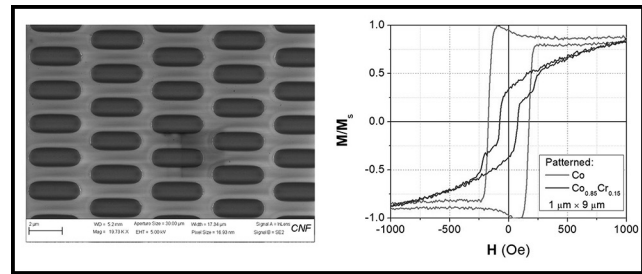


Figure 3: (a) SEM image of lithographically patterned Co. (b) Magnetic hysteresis loops of similarly patterned Co and CoCr.

to program dipole orientations in individual magnetic panels, enabling more complex modes of actuation for executing specific tasks. In order to achieve magnetic writing capabilities, we must define the appropriate combination of magnetic materials and writing technique. Using the AJA magnetron sputterer in CNF, we have investigated materials such as Co, CoCr alloys, and Co/Pt multilayers and measured their magnetic properties via vibrating sample magnetometry (VSM) and magnetic force microscopy (MFM). Additionally, we have patterned these films to understand the effects of shape anisotropy on their magnetic properties (Fig.3).

We are currently using these results to determine viable approaches for magnetic recording. One promising method would rely on the disparity of the in-plane coercivity between Co and CoCr. One could use a large field to orient Co, a high coercive field material, in one direction, and subsequently use a smaller field to write CoCr, a softer material, in the opposite direction without affecting the Co. Leveraging shape anisotropy, one could repeat this process along an orthogonal axis to achieve four unique magnetic orientations. This simple magnetic writing scheme for magnetic panels combined with a flexible and robust exoskeleton deposited using ALD would facilitate the design of microscopic actuating systems for smart self-assembly and robotics.

References:

- [1] K. J. Dorsey, T. G. Pearson, E. Esposito, S. Russell, B. Bircan, Y. Han, M. Z. Miskin, D. A. Muller, I. Cohen, P. L. McEuen, *Adv. Mater.* 2019, 31, 1901944.
- [2] J. Cui, T. Huang, Z. Luo, P. Testa, H. Gu, X. Chen, B. J. Nelson, L. J. Heyderman, *Nature* 2019, 575, 164.
- [3] R. Niu, C. X. Du, E. Esposito, J. Ng, M. P. Brenner, P. L. McEuen, I. Cohen, *PNAS* 2019, 116 (49), 24402.

Water Propagation on a Surface with Buried Nanochannels

CNF Project Number: 2123-12

Principal Investigator(s): Shalabh C. Maroo

User(s): Sajag Poudel, An Zou, Manish Gupta

Affiliation(s): Department of Mechanical and Aerospace Engineering, Syracuse University, Syracuse, NY 13244

*Primary Source(s) of Research Funding: National Science Foundation Career Award NO. 1454450,
Office of Naval Research Grant NO. N000141812357*

Contact: scmaroo@syr.edu, sapoudel@syr.edu, azou@syr.edu, magupta@syr.edu

Website: <http://maroo.syr.edu>

Primary CNF Tools Used: Heidelberg mask writer (DWL 2000), manual photoresist spinner, Gamma coat-develop tool, GCA auto stepper, ASML stepper, YES image reversal oven, ABM contact aligner, SÜSS MA6-BA6 contact aligner, e-beam evaporator, Oxford PECVD, GSI PECVD, Glen 1000 Plasma, Anatech resist strip, Oxford 81/82 etcher, Oxford 100 etcher, Plasma-Therm deep silicon etcher, Unaxis 770 deep silicon etcher, optical microscope, scanning electron microscope, atomic force microscope

Abstract:

We investigated the wicking of a finite water drop sitting on a surface with well-defined cross-connected buried nanochannels by experiments and analytical models. The wicking process is composed of wicking-dominant and evaporation-dominant regimes, with each further divided into two subregimes. The wicking is initially governed by surface tension and viscous forces, and later by hydrodynamic dissipation within the droplet sitting on the top surface due to the finite liquid supply. The work reported here is part of a journal article published in *Journal of Physical Chemistry C* [1].

Summary of Research:

Wicking is the phenomenon in which liquid propagates in a porous medium primarily due to the surface tension, curvature, and the solid-liquid intermolecular attraction force. Wicking plays a significant role in various areas, such as thin film evaporation, printing, oil processing, etc. Superior wickability of a porous medium is a major motivation to employ them in phase-change heat transfer applications, which is widely accepted as one of the most promising solutions to the increasing demand of high heat flux removal. Here, we present an experimental work of water propagation on a surface with buried nanochannels. The geometry of the nanochannel being well controlled and defined makes it a perfect candidate to conduct such investigation due to: (1) accurately modeled capillary pressure without having to predict the meniscus shape; and (2) easily achieved long wicking distance as the evaporation is hindered.

The buried cross-connected nanochannels were fabricated on a silicon (Si) substrate by etching patterned sacrificial metal layers buried under a 300 nm thick

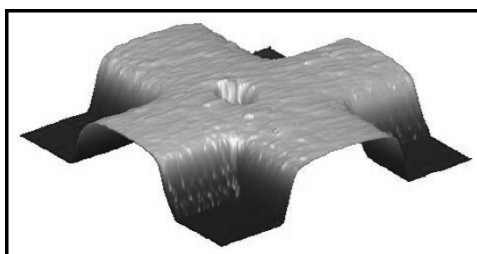


Figure 1: Atomic force microscope (AFM) image of the profile of channels and pores.

silicon dioxide (SiO_2) film from plasma enhanced chemical vapor deposition (PECVD). The channel geometry was determined by the pattern of sacrificial layers, which was attained by a lift-off process. The cross-connected channels, made from two sets of channels perpendicular to each other, allow for ease of liquid exchange inside the channels. Further, at each intersect of the channels, a 2 μm pore was fabricated allowing liquid present above the surface to flow into the channels. Figure 1 shows an atomic force microscope (AFM) image of the surface (channel width: 5 μm , spacing: 5 μm , height: 728 nm).

In wicking experiments, the spreading of a 2- μL water droplet on a sample with buried nanochannels was recorded using a high speed camera. The volume of the droplet was generated and controlled by a string pump. Using a vertical-translation stage, the sample was raised until it touched the droplet, after which the droplet starts to spread on the surface, as well as wick into the channels before eventually drying out due to evaporation. The water propagation during wicking were characterized by three parameters: wicking radius

(R_w , defined as radius of the entire wetted area), droplet base radius (R_d , defined as radius of the droplet sitting above nanochannels), and wicking distance (w_d , defined as difference between above two). Figure 2 shows a schematic of these parameters. Both R_w and R_d were obtained from image analysis of the high-speed video and were measured with time.

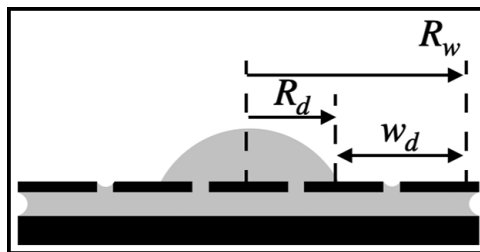


Figure 2: Schematic of definition of wicking radius (R_w) and droplet base radius (R_d).

Figure 3 shows the evolution of R_w and R_d . The wicking process can be divided into two distinct regimes: initial wicking-dominant (regime I) and later evaporation-dominant regime (II). Each of these two regimes can be further divided into two subregimes. When the droplet comes in contact with the surface (defined as $t = 0$), it spreads on the top of the surface immediately; water starts wicking into the channels as well, causing both R_d and R_w to increase fast in the first subregime I-A. The end of subregime I-A is defined by the time ($t = t_d$) when R_d reaches its maximum. In subregime I-B, the water menisci in the channels continues to advance radially outward and reaches a maximum wicking radius at $t = t_{max}$; while the R_w remains nearly constant during this period. Beyond t_{max} , the wicking process transitions to regime II where evaporation dominates, causing the meniscus front recede and dry out eventually due to the finite water supply from the droplet.

In subregime II-A, the water evaporated from menisci in the channels and pores is balanced by the water supply from the droplet, leading to a nearly constant R_w . The R_d maintains at its maximum as well, with a decrease in droplet height due to the shrink in volume. After the droplet height reaches a certain minimum value, water front above nanochannels starts to recede, leading to a decreased R_d and therefore subregime II-B

where evaporation flux in menisci in channels overwhelms water supply from the droplet, causing R_w to decrease and eventually dry out.

The data of wicking distance (w_d) in regime I are in good agreement with two analytical models which can be used to predict wicking distance evolution in nanochannels. In regime I-A, the w_d can be predicted by Xiao's model

[2] where the flow is governed by surface tension (flow driving force) and viscous forces (flow resistance) with unlimited liquid supply. Due to the finite droplet volume, the w_d deviates from this prediction in regime I-B, but is in good agreement with prediction from Ruijter's model [3], where the hydrodynamic dissipation within droplet was considered as the dominant reason behind the loss of surface during spreading.

Conclusions and Future Steps:

The wicking in buried nanochannels is composed of wicking-dominant and evaporation-dominant regimes. The wicking is initially governed by surface tension and viscous forces, and later by hydrodynamic dissipation within the droplet sitting on the top surface.

References:

- [1] S. Poudel, A. Zou, S.C. Maroo, J. Phys. Chem. C, 123: 23529-23534 (2019).
- [2] R. Xiao, R. Enright, E.N. Wang, Langmuir, 26: 15070-075 (2010).
- [3] M.J. de Ruijter, J. De Coninck, G. Oshanin, Langmuir, 15: 2209-2216 (1999).

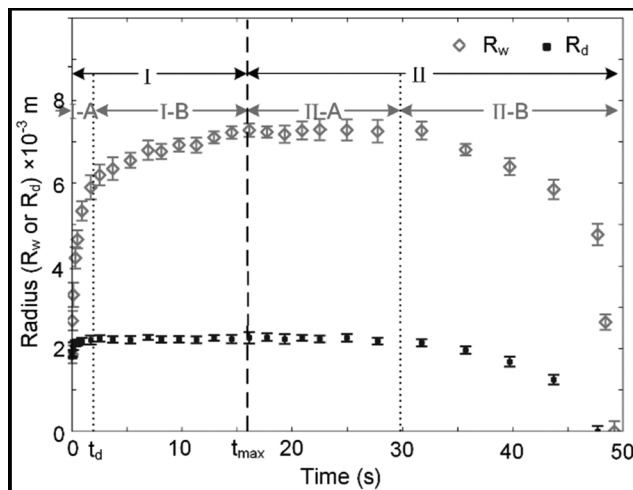


Figure 3: Evolution of wicking radius (R_w) and droplet base radius (R_d) for wicking of 2 μ l droplet.

Quantum Optomechanical Coupling in Hexagonal Boron Nitride Membranes

CNF Project Number: 2126-12

Principal Investigator(s): Gregory D. Fuchs

User(s): Nikhil Mathur

Affiliation(s): Applied and Engineering Physics, Cornell University

Primary Source(s) of Research Funding: National Science Foundation (DMR-1719875)

Contact: gdf9@cornell.edu, nm648@cornell.edu

Website: <http://fuchs.research.engineering.cornell.edu/>

Primary CNF Tools Used: Heidelberg DWL2000, ASML DUV stepper, Oxford 81 etcher, P10 profilometer, SC4500 evaporator, Zeiss scanning electron microscope (SEM)

Abstract:

We report on the fabrication, electrostatic actuation, and optical detection of micro-mechanical resonator devices composed of a hexagonal boron nitride (hBN)/graphene membrane covering a 285 nm-deep circular hole. The mechanical resonant frequency of the fundamental mode is 11 MHz, with a Q factor of 2000. We also used a focused ion beam (FIB) to create defects in suspended hBN membranes and then used confocal laser-scanning microscopy to study single-photon photoluminescence from the exposed regions. By resonantly driving a membrane in which quantum emitters are embedded, we hope to take advantage of strong defect-strain coupling to explore the physics of a hybrid quantum system.

Summary of Research:

Solid-state single-photon sources are an essential component of emerging quantum technologies. Point defects in hBN are a bright source of single-photons at room temperature with interesting coupling to strain in the crystal. This strong coupling has been used to statically tune defect emission [1,2] and it gives hBN the potential to be used in a hybrid quantum system entangling single photons with single phonons [3].

To study the dynamic optomechanical coupling of an hBN defect to a driven membrane, we first design devices that achieve high strain through electrostatic actuation.

To fabricate these devices, we use DUV photolithography to etch a pattern of holes and trenches into SiO_2 and then align a second layer of patterned photoresist to evaporate Ti/Au electrodes at the top and bottom of the holes. Figure 1 shows a scanning electron micrograph of such a device before transferring the heterostructure membrane over the electrodes. After the photolithography, we use a polymer-assisted exfoliation method to transfer a multilayer hBN/graphene heterostructure over the hole such that the graphene is in contact with only the top electrodes and suspended above the bottom electrode (Figure 2). By applying voltage across the electrodes, the electrostatic force deflects the suspended membrane and

the induced strain shifts the optical transition energy of defects within the hBN flake.

We detect motion of the membrane using interferometric techniques by focusing a 637 nm laser onto the center of the membrane while the device is under high vacuum ($< 10^{-5}$ Torr). When the membrane is vibrating, the optical phase difference created by

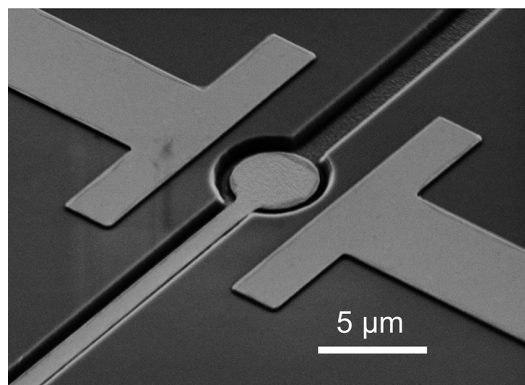


Figure 1: SEM of the fabricated device substrate onto which the heterostructure membrane was transferred. The trenches are etched 285 nm into the SiO_2 substrate and a 30 nm film of Ti/Au is evaporated to define the electrodes.

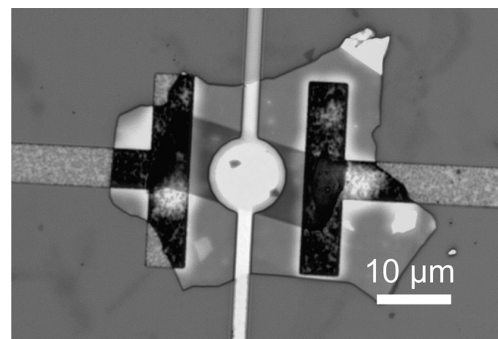


Figure 2: Optical micrograph of a 25 nm thick hBN/graphene heterostructure membrane exfoliated onto the device substrate. (See pages vi-vii for full color version.)

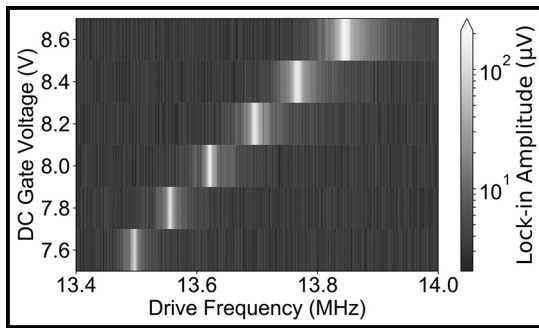


Figure 3: Lock-in sweep data showing the mechanical resonance at varying DC offset voltages.

the gap between the membrane and bottom electrode fluctuates and thus so does the reflection intensity. We direct the reflected light onto a high-frequency photodiode, whose voltage is the input to a lock-in amplifier with the electrostatic drive as the reference. When we sweep the driving frequency while monitoring the lock-in signal, we detect the fundamental resonant mode at around 11 MHz. Additionally, by applying a DC offset, the static pre-tension can be used to tune the resonant frequency and improve the resonator Q factor (Figure 3).

Although much progress has been made in creating optically stable defects in hBN, most methods produce emitters at random positions [4]. To integrate and couple the emitters with other structures, defects must be created with nanometer precision and reproducible properties. We have made significant progress on this front by producing arrays of quantum emitters at deterministic locations. Using a gallium FIB [5], we mill shallow circular pits 300 nm across and 5 nm deep on exfoliated hBN (Figure 4a), suspended over trenches to avoid background fluorescence induced by the substrate. We then anneal the devices for 30 minutes at 850°C in a N_2 environment.

Using a confocal laser-scanning microscope, we measure photoluminescence from the milled regions (Figure 4b). Upon close inspection, we observe high-purity single-photons from several defect-based emitters close to the perimeter of each milled circle. Autocorrelation statistics from one of these quantum emitters is shown in Figure 4c.

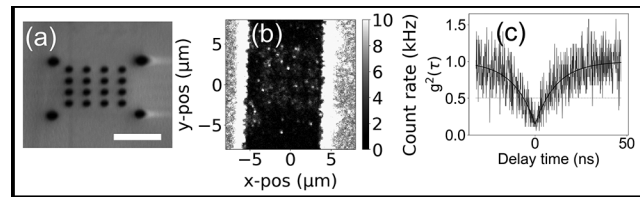


Figure 4: a) SEM of a suspended multilayer hBN membrane, patterned with an array of circular pits milled using a gallium FIB. Scale bar is 5 μm . b) Photoluminescence map of FIB-exposed region. c) Second-order autocorrelation function of the emission from an isolated defect, fit to a two-level model. The measurement of $g^2(\tau = 0) < 0.5$ indicates that the source is emitting single-photons.

Conclusions and Future Steps:

While driving on resonance, we will be able to scan the interferometry laser position over the entire membrane and achieve high spatial resolution of the mechanical mode. We can then infer the strain profile using a finite element model of the device. We will then create isolated point defects in the hBN using the FIB method discussed and will be able to quantify the shift in the optical transition, elucidating the potential for hBN to be used in quantum optomechanical devices.

References:

- [1] N. Mendelson, M. Doherty, M. Toth, I. Aharonovich, T. T. Tran, "Strain-Induced Modification of the Optical Characteristics of Quantum Emitters in Hexagonal Boron Nitride" *Adv. Mater.* 2020, 1908316 (2020).
- [2] G. Grosso, H. Moon, B. Lienhard, S. Ali, D. K. Efetov, M. M. Furchi, P. Jarillo-Herrero, M. J. Ford, I. Aharonovich, and D. Englund, "Tunable and high purity room-temperature single photon emission from atomic defects in hexagonal boron nitride" *Nat. Commun.* 8, 705 (2016).
- [3] X. Guo, Z.-Q. Yen, T. Li, "High-speed quantum transducer with a single-photon emitter in an atomically thin resonator" *arXiv:1712.09245* (2017).
- [4] I. H. Abidi, N. Mendelson, T. T. Tran, A. Tyagi, M. Zhuang, L. T. Weng, B. Özyilmaz, I. Aharonovich, M. Toth, Z. Luo, "Selective Defect Formation in Hexagonal Boron Nitride" *Adv. Opt. Mater.* 7, 1900397 (2019).
- [5] J. Ziegler, R. Klaiss, A. Blaikie, D. Miller, V. R. Horowitz, B. J. Alemán, "Deterministic Quantum Emitter Formation in Hexagonal Boron Nitride via Controlled Edge Creation" *Nano Lett.* 19, 3, 2121-2127 (2019).

Making a Microfluidic Device to Mimic Flow Through Porous Medium

CNF Project Number: 2385-15

Principal Investigator(s): Brian Kirby

User(s): Katherine Polhemus

Affiliation(s): Mechanical and Aerospace Engineering, Cornell University

Primary Source(s) of Research Funding: IGERT Program for Earth Energy

Contact: kirby@cornell.edu, kcp44@cornell.edu

Primary CNF Tools Used: CAD software L-Edit, hot press, CorSolutions Microfluidic Probe Station

Abstract:

With the rapid depletion of known oil reserves, detecting properties of the oil reservoirs and optimizing oil extraction is critical. By measuring the aqueous properties of the reservoirs, decisions can be made on which reservoirs to drill and the available quantity of oil to extract, with minimal environmental impact. Utilizing particles in testing can provide a variety of information about the reservoir. The objective of the proposed work is to characterize the behavior of particles at the oil-water interface in order to optimize their use as subsurface sensors. In order to complete the optimization, a microfluidic model for the environment needs to be developed. This past year's work involves making microfluidic devices to mimic water flowing through the subsurface and oil trapped in pores. The design and mold to make the mold was developed in the CNF first using photolithography to create a mold with negative photoresist which was used to make microfluidic channels out of polydimethylsiloxane and later using positive photoresist and etching to create a mold to make microfluidic channels out of polypropylene.

Summary of Research:

The work in the CNF has consisted of using micro-fabrication techniques to make a microfluidic device. Using the CAD software L-Edit to make patterns to transfer to a mask using the Heidelberg mask writer, in the past year, we have made two types of masks: one for positive photoresist and the other for negative photoresist. The first set of microfluidic devices used the negative photoresist (SU-8) to make a mold. The process of making a mold with photoresist (photolithography) consist of the steps; 1) Pour and spin photoresist onto a wafer (using CNF spinner), 2) Bake photoresist (using CNF hot plates), 3) Wait time, 4) Expose photoresist (using ABM contact aligner), 5) Second wait time, 6) Development of photoresist.

At the end of the process, we have a mold out of SU-8 on top of a wafer. In the Kirby research group's lab, we made microfluidic devices by pouring PDMS on top of the mold and baking, then attaching, the molded PDMS to a glass slide through plasma cleaning. Unfortunately for our application, we need the PDMS to be very

hydrophobic and PDMS was not hydrophobic enough for the experiments. Therefore, we switched to making devices out of a polypropylene — a much more hydrophobic material. To make molded polypropylene pieces we used hot embossing, which is done on the CNF hot press.

Because of the large pressure applied during embossing, we needed a stronger mold than SU-8, so we switched to making molds out of silicon. To make a mold out of silicon, a positive photoresist is spun instead of negative and after the photolithography process, the wafer is etched on the deep reactive ion etcher in the CNF. The mold is used in the CNF hot press to hot emboss the pattern onto polypropylene. Another piece of polypropylene is pressed to a thinner thickness using the using the hot press. Finally, the device is bonded together using the hot press. We also used the CorSolutions Microfluidic Probe Station as a connection method for tubes to the device, which allowed us to flow oil and particles into the device.

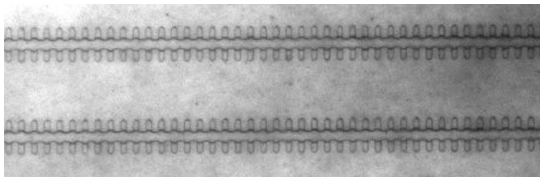


Figure 1: Oil-water contact line in polypropylene device.

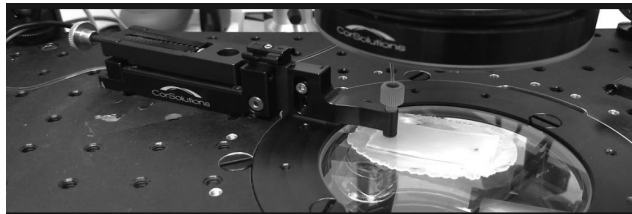


Figure 2: Device on CorSolution station.



Figure 3: Etched silicon mold for hot pressing.

The Role of Smart Water in Oil Recovery

CNF Project Number: 2385-15

Principal Investigator(s): Brian Kirby

User(s): Julia Radzio

Affiliation(s): Mechanical and Aerospace Engineering, Cornell University

Primary Source(s) of Research Funding: Cornell Engineering Learning Initiatives (ELI)

Contact: kirby@cornell.edu, jr932@cornell.edu

Website: <http://blogs.cornell.edu/kirbyresearch/>

Primary CNF Tools Used: CRC hot press, CorSolutions Microfluidic Probe Station

Abstract:

Global oil demand and consumption continues to increase yearly, but current oil recovery techniques lack the efficiency needed to extract most of the oil in reservoirs. The use of nanoparticles as sensors for the available quantity of oil to extract has been demonstrated in experimental laboratory evaluations with core samples. This report will discuss how microfluidic devices were used to provide a controlled environment for studying how particles partitioned between oil and flooding fluids. Smart water was injected into the devices at various flow conditions in order to determine favorable circumstances for particles to enter the pockets of the channels. Solutions that contained less than 50% water to ethanol minimized particle clogging at the inlets and T-intersections of the devices. At 2.5 $\mu\text{L}/\text{min}$, the contact line between the oil and smart water remained stable and boluses did not appear. The hydrophobicity of the walls of the inlets negatively affected the flow of particles in smart water solutions. These flow conditions will ultimately allow for the particle concentration at the inlet and outlet of microfluidic devices to be measured, which will inform the effectiveness of particles as sensors for oil in a reservoir.

Summary of Research:

With the rapid depletion of known oil reserves, detecting properties of oil reservoirs and optimizing oil extraction is critical. Global oil demand and production continues to increase every year, with the rate of oil consumption in 2018 having grown to an above average 1.4 million barrels per day [1]. Nanoparticles can serve as sensors for the interiors of oil reservoirs by partitioning into oil or releasing nanoreporters upon contact with oil [2]. Microfluidic devices can provide a micro-scale environment to analyze singular effects in pores by modeling partially saturated rock with crude oil [3]. Laminar flow in the microchannels of the devices allows for experiments that can be reliably repeated and observed over a pore network [3].

The microfluidic device that is utilized to mimic subsurface conditions is fabricated from two layers of polypropylene in the Cornell NanoScale Facility. To manufacture a mold for forming the channels, a Si wafer is patterned with SPR-220-7 using standard photolithography techniques and deep reactive ion etching. The mold is used to emboss a polypropylene square on a CRC Hot Press at 166.6°C at 200 lbf (pound-force) for 2.5 minutes, after which the embossed piece is bonded to blank polypropylene square with a thickness between 0.17 mm and 0.24 mm at 149.5°C at 9 lbf above

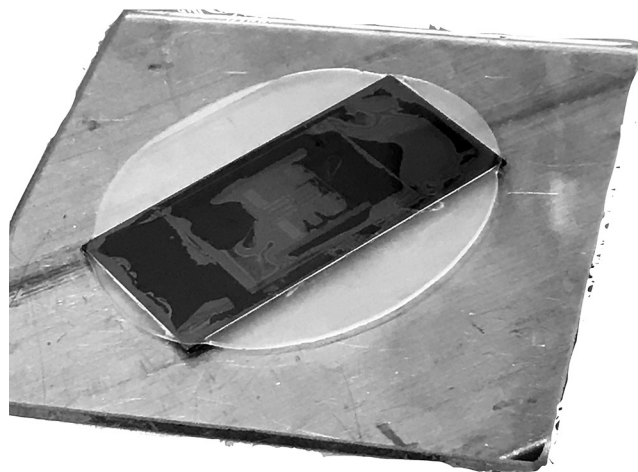


Figure 1: Silicon wafer patterned with 16 channel design.

the baseline force for six minutes. As seen in Figure 1, the design features 16 parallel, bifurcating channels that allow for uniform, low flow rates for the given syringe pump range. The depth and width of the main channels was approximately 20 μm , and the pockets were rounded with a side width of 13 μm and placed apart from each other every 13 μm .

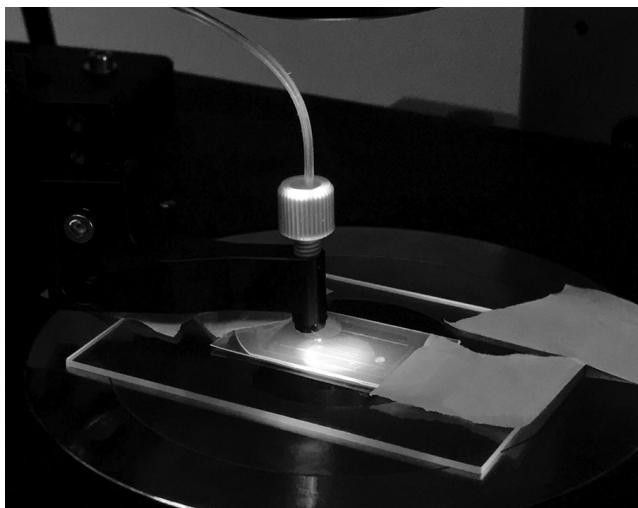


Figure 2: Experimental setup close-up of CorSolutions arm connector.

The formation of oil boluses in the inlet of the microfluidic devices after water-ethanol solutions were injected was investigated. Boluses that formed at any point in the device would lead to particles dispersing at an uneven rate and would lead to clogs in the channels of the device. Undecane, oil, and water-ethanol were sequentially injected into a device using a Tygon® tube as shown in Figure 2 (CorSolutions). Boluses at the inlet were qualified as a distinct second phase that appeared to fill the center of the inlet or as singular bubbles of oil that remained attached to the inlet wall for the duration of the trial as seen in Figure 3.

For every flow rate, 25% water: 75% ethanol had inlets free of boluses. The contact line between oil and the injected solution was most stable for 2.5 $\mu\text{L}/\text{min}$, as it took the longest amount of time for the oil to be displaced from the pockets compared to 5 and 10 $\mu\text{L}/\text{min}$. The 25% water: 75% ethanol solution containing microparticles was injected in a new device at 10 $\mu\text{L}/\text{min}$. 2 μm particles clumped together immediately at the inlet and the first T-intersection for all three trials as shown in Figure 4, but there was no evidence of boluses in the inlet.

Conclusions and Future Steps:

Because the devices were primed with oil, it was expected that the particles would partition from the

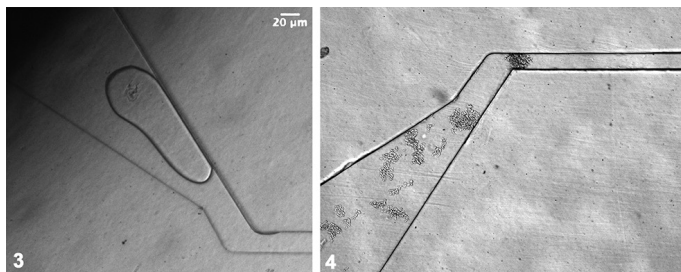


Figure 3, left: Oil bolus attached to wall of inlet of microfluidic device.
Figure 4, right: Particles clustered at the narrowing of the inlet for 25% water: 75% ethanol solution.

injected solution to the oil in the pockets. As the particles had a tendency to attach to the walls of the inlet and to each other at T-intersections, no particles were able to flow into the channels of the devices at a variety of water-ethanol solutions and flow rates. Qualitative data presented in this report suggests that smart water consisting of 25% de-ionized water and 75% ethanol prevents boluses from forming in the inlet of the device. However, the hydrophobicity of the solution and the surface of the channels causes particles to cluster at the inlet and clog flow into the channels.

Future work will focus on changing the composition of the smart water with a surfactant that allows particles to partition into the oil in the pockets, and ultimately serve as a sensor for oil.

References:

- [1] British Petroleum. (2019). BP Statistical Review of World Energy 2019. (Report No. 68).
- [2] Siresha, M., Babu, V. J., Kiran, S. K., and Ramakrishna, S. (2018). A Review on Nanomaterial Revolution in Oil and Gas Industry for Enhanced Oil Recovery Methods. Res Dev Material Sci. 4 (1).
- [3] Gogoi, S., and Gogoi, S. B. (2019) Review on microfluidic studies for EOR application. Journal of Petroleum Exploration and Production Technology.

Atomically Thin Actuator-Enabled Micro-Machines and Micro-Structures

CNF Project Number: 2416-16

Principal Investigator(s): Itai Cohen, Paul L. McEuen

User(s): Qingkun Liu, Wei Wang, Baris Bircan, Michael F. Reynolds

Affiliation(s): Kavli Institute at Cornell for Nanoscale Science, School of Applied and Engineering Physics, Laboratory of Atomic and Solid-State Physics, Department of Physics; Cornell University

Primary Source of Research Funding: National Science Foundation Grant DMR-1719875; DMR-1435829 Army Research Office Grant W911NF-18-1-0032

Contact: itai.cohen@cornell.edu, plm23@cornell.edu, ql59@cornell.edu, ww459@cornell.edu, bb625@cornell.edu

Primary CNF Tools Used: Oxford ALD FlexAL, Arradiance ALD Gemstar-6, Oxford 81/100 etchers, ABM contact aligner, SC 4500 odd-hour, AJA sputter, AJA ion mill, Oxford Cobra ICP etcher, Heidelberg DWL2000

Abstract:

The ability to actuate an object at the microscale is an important technological aspect of manufacturing micro-robots and micro-machines. Here we demonstrate that micro-actuators made by atomically thin layers of metals and dielectrics could bend in response to electrical or chemical signals. The electrical micro-actuators could work in both volatile and shape memory regimes depending on the applied voltages, enabling electrically programmable three-dimensional structures and artificial cilia. The chemo-responsive actuators allow for self-folding three-dimensional origami structures activated by the pH of the aqueous solution.

Summary of Research:

Our team has developed atomically thin actuators that can bend in response to electrical and chemical stimuli. This approach makes it possible to create complex structures, machines, and microrobots by using origami design principles at the microscale.

Our team first discovered a microscale multistable electrochemical shape memory actuator that “memorizes” a continuous range of shapes, which is distinct from only one or two stable shapes of the conventional shape memory materials associated with the transformation of crystal structures [1]. The core of the device comprises of an electrochemically active platinum membrane capped on one side by an inert layer (Figure 1a). To achieve a continuous range of shapes, the team developed a technique based on applying voltage to shift the electrochemical balance between platinum and a surrounding electrolyte in order to drive oxygen ions through one surface of the platinum membrane (Figure 1b). This electrochemical redox reaction of platinum creates a differential in stress between the two sides of the actuator, causing the structure to cycle and maintain a submicron bending radius for a long time (Figure 1c-f).

This electrical programmability of nanometer-thin membranes can be harnessed to create three dimensional shapes that can be reversibly erased and

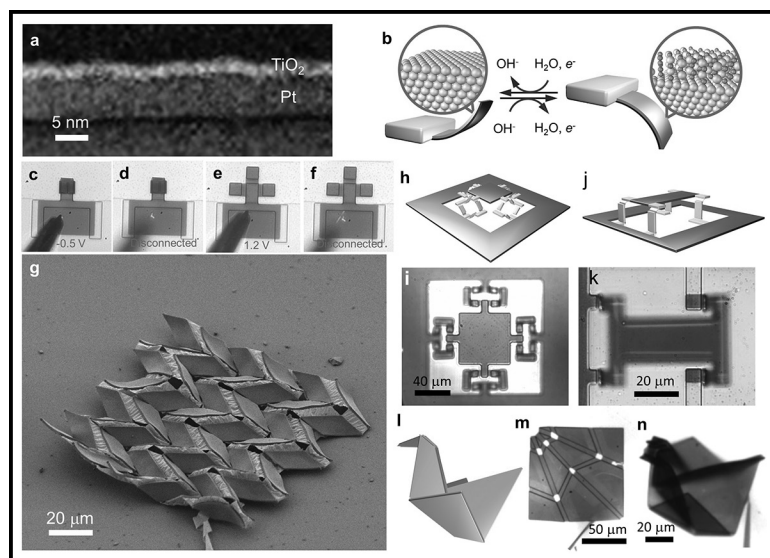


Figure 1: Electrically programmable shape memory actuator-enabled micro-devices. (See cover for Figure 1g in full color. Used with permission.)

rewritten by short electrical pulses. We then localized the bending position by patterning rigid polymeric panels (Figure 1g). Origami principle could be employed to design micro-machines owing to the capability of the bidirectional folding of actuators by reversing the deposition order of the platinum and inert layers. We demonstrate electrically reconfigurable micro-origami motifs and bistable microactuators (Figure 1h-n).

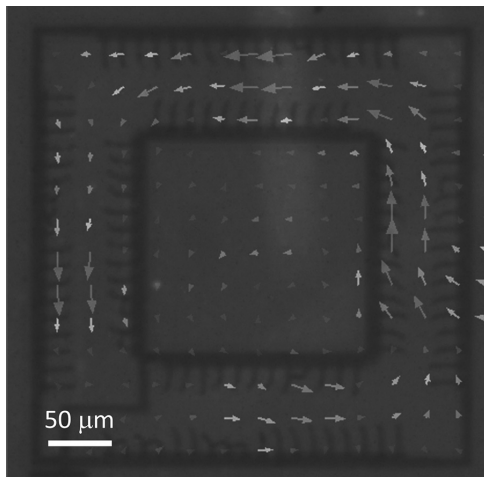


Figure 2: Electrical artificial cilia-pumped flow pattern with its direction indicated by arrows. (See pages vi-vii for full color version.)



Figure 3: A spacer Miura-ori fold made using ultra-thin, self-folding atomic layer deposited sheets.

The manufacturing process is fully compatible with the microelectronic fabrication technology, making it easy to integrate with control circuit. These results could lead to new micro- or nano- electromechanical systems for robotic applications.

Besides the shape memory effect, the atomically thin platinum/titanium membrane could work as a volatile actuator. The actuators bend due to the difference in stress between the platinum and titanium layers that stems from the electrochemical adsorption of oxygen species on the surface of platinum. By harnessing this new type of electrical micro-actuator, our team developed electrically controllable artificial cilia that efficiently pump fluid in a steady unidirectional flow (Figure 2).

Individually addressable micro-scale robotic cilia have the potential to enable unprecedented control over microfluidic environments. They could be used to sort microscale particles, control chemical reactions, and transport viscoelastic materials. Such systems could also be used to better understand biological processes such as neurotransmitter transport in the brain, as well as clearing in the liver and lungs. The electrical nature of these artificial cilia makes it possible to integrate control circuits and power sources, allowing for sequential and addressable generation of arbitrary flow patterns. We envision that this technology will find broad applications. For example, in addition to ushering unparalleled control of fluids moving over surfaces, such electrically programmable artificial cilia could serve as actuators for aquatic microscale robots.

Our team also developed chemo-responsive micro-actuators that enable self-folding three-dimensional micro-architectures using origami principle. The mapping of an arbitrary three-dimensional shape to an origami fold pattern requires the assignment of fold angles ranging from -180° to $+180^\circ$. Therefore,

bidirectional folding action is essential in creating a complete platform for origami-based self-assembly.

Our previous work achieved unidirectional folding with atomically thin sheets of hard materials [2], but could not be used to fabricate complex geometries that required bidirectional folding. To address this problem, our team has developed a scalable microfabrication process to create microscale bidirectional folds using 4 nm thick atomic layer deposition SiN_x - SiO_2 bilayer films [3]. Strain differentials within these bilayers result in bending, producing microscopic radii of curvature. To take advantage of this intrinsic curvature, we photolithographically pattern these bilayers and localize the bending using 1 μm thick panels of rigid SU-8 polymer. This allows us to fabricate a variety of complex micro-origami devices, ranging from relatively simple geometries with six folds to more complex ones with nearly 100 folds, such as the spacer Miura-ori fold seen in Figure 3.

Upon release, these devices self-fold according to prescribed patterns. Our approach combines automated lithography mask design with easily scalable planar microfabrication methods, making it easy to fabricate and deploy micro-origami devices en masse. This work has been compiled into a manuscript and submitted for publication.

References:

- [1] Liu, Q., Wang, W., Reynolds, M., Miskin, M., Cao, M. C., Muller, D. A., McEuen, P. L. Cohen, I., Electrically Programmable Micro-Scale Shape Memory Devices, APS March Meeting, 2020.
- [2] Miskin, M., Dorsey, K., Bircan, B., Han, Y., Muller, D., McEuen, P., and Cohen, I. Graphene-based bimorphs for micron-sized autonomous origami machines. Proceedings of the National Academy of Sciences, 115: 466-470 (2018).
- [3] Bircan, B., Miskin, M., Dorsey, K., McEuen, P. and Cohen, I., Bidirectional Folding with Nanoscale Sheets for Autonomous Micro-Origami, 2018.